Received: 9 January 2021 | Revised: 13 September 2021 | Accepted: 17 September 2021

DOI: 10.1002/psp4.12717

ARTICLE

Unraveling pleiotropic effects of rifampicin by using physiologically based pharmacokinetic modeling: Assessing the induction magnitude of P-glycoprotein–cytochrome P450 3A4 dual substrates

Xian Pan[1] | **Shinji Yamazaki**[2] | **Sibylle Neuhoff**[1] | **Mian Zhang**[1] | **Venkatesh Pilla Reddy**[3,4]

[1]Simcyp Division, Certara UK Limited, Sheffield, UK

[2]Pharmacokinetics, Dynamics & Metabolism, Pfizer Worldwide Research & Development, San Diego, California, USA

[3]Modelling and Simulation, Early Oncolog, Oncology R&D, AstraZeneca, Cambridge, UK

[4]Clinical Pharmacology and Pharmacometrics, Biopharmaceuticals R&D, AstraZeneca, Cambridge, UK

Correspondence
Venkatesh Pilla Reddy, Clinical Pharmacology and Pharmacometrics, Biopharmaceuticals R&D, Aaron Klug Building, Granta Park, Cambridge CB21 6GH, UK.
Email: Venkatesh.Reddy@astrazeneca.com
and
Sibylle Neuhoff, Simcyp Division, Certara UK Limited, Sheffield, S1 2BJ, UK.
Email: sibylle.neuhoff@certara.com

Present address
Shinji Yamazaki, Drug Metabolism & Pharmacokinetics, Janssen Research & Development, LLC, San Diego, California, USA

Funding information
No funding was received for this work.

Abstract

Rifampicin induces both P-glycoprotein (P-gp) and cytochrome P450 3A4 (CYP3A4) through regulating common nuclear receptors (e.g., pregnane X receptor). The interplay of P-gp and CYP3A4 has emerged to be an important factor in clinical drug–drug interactions (DDIs) with P-gp–CYP3A4 dual substrates and requires qualitative and quantitative understanding. Although physiologically based pharmacokinetic (PBPK) modeling has become a widely accepted approach to assess DDIs and is able to reasonably predict DDIs caused by CYP3A4 induction and P-gp induction individually, the predictability of PBPK models for the effect of simultaneous P-gp and CYP3A4 induction on P-gp-CYP3A4 dual substrates remains to be systematically evaluated. In this study, we used a PBPK modeling approach for the assessment of DDIs between rifampicin and 12 drugs: three sensitive P-gp substrates, seven P-gp–CYP3A4 dual substrates, and two P-gp–CYP3A4 dual substrates and inhibitors. A 3.5-fold increase of intestinal P-gp abundance was incorporated in the PBPK models to account for rifampicin-mediated P-gp induction at steady state. The simulation results showed that accounting for P-gp induction in addition to CYP3A4 induction improved the prediction accuracy of the area under the concentration-time curve and maximum (peak) plasma drug concentration ratios compared with considering CYP3A4 induction alone. Furthermore, the interplay of relevant drug-specific parameters and its impact on the magnitude of DDIs were evaluated using sensitivity analysis. The PBPK approach described herein, in conjunction with robust *in vitro* and clinical data, can help in the prospective assessment of DDIs involving other P-gp and CYP3A4 dual substrates. The database reported in the present study provides a valuable aid in understanding the combined effect of P-gp and CYP3A4 induction during drug development.

Study Highlights

WHAT IS THE CURRENT KNOWLEDGE ON THE TOPIC?

Rifampicin is a well-known agonist of the pregnane X receptor (PXR). Both cytochrome P450 3A4 (CYP3A4) and P-glycoprotein (P-gp) can be upregulated by rifampicin via the PXR pathway. Although CYP3A4 induction can be readily accounted for by physiologically based pharmacokinetic (PBPK) modeling, P-gp induction is seldom addressed.

WHAT QUESTION DID THIS STUDY ADDRESS?

This study systematically evaluated the utility of a PBPK modeling approach to predict oral exposure of three sensitive P-gp substrates and nine P-gp–CYP3A4 dual substrates by accounting for P-gp and CYP3A4 induction simultaneously.

WHAT DOES THIS STUDY ADD TO OUR KNOWLEDGE?

PBPK modeling and simulation with the data set presented herein demonstrated that accounting for intestinal P-gp induction by incorporating a relative expression factor of 3.5 significantly improved DDI predictions for P-gp–CYP3A4 dual substrates coadministered with rifampicin.

HOW MIGHT THIS CHANGE DRUG DISCOVERY, DEVELOPMENT, AND/OR THERAPEUTICS?

The PBPK modeling approach described herein, in conjunction with robust *in vitro* and clinical data, can help in the prospective assessment of DDIs of new chemical entities that are P-gp and CYP3A4 dual substrates and inducers. The database reported in the present study provides a valuable aid in understanding the effect of simultaneous induction of P-gp and CYP3A during drug development.

INTRODUCTION

Physiologically based pharmacokinetic (PBPK) modeling has been widely used in the assessment of drug–drug interactions (DDIs) during the past decade.[1–3] Although the prediction of competitive inhibition of cytochrome P450 (CYP) enzymes remains one of the most established areas of PBPK modeling, there has been an increase in the application and regulatory acceptance of the use of PBPK in predicting DDIs with other mechanisms such as CYP induction and competitive inhibition of drug transporters.[4,5]

P-glycoprotein (P-gp), a well-studied adenosine triphosphate–binding cassette transporter, is an efflux pump expressed on the apical membranes of various types of cells, such as hepatocytes, renal proximal tubular cells, brain capillary endothelial cells, and gut enterocytes.[6–8] Given the localization of P-gp in these organs, it functions to facilitate biliary clearance and active renal secretion while limiting penetration of drugs across the blood–brain barrier and restricting absorption of drugs into gut enterocytes from the gut lumen. As the broad substrate specificity of P-gp considerably overlaps with that of CYP3A, it has been suggested that P-gp and CYP3A often work together, in particular in oral drug absorption, to limit the systemic exposure of their substrates.[9–11] In addition to being functionally synergistic, P-gp and CYP3A are also shown to be coregulated via the pregnane xenobiotic receptor (PXR) and the constitutive androstane receptor (CAR), therefore agonists of these nuclear receptors may have the potential to induce P-gp and CYP3A simultaneously.[12] Given the commonality in the mechanisms of P-gp and CYP3A induction, the US Food and Drug Administration (FDA) recommends that clinical findings on CYP3A induction can be used to inform decisions about whether a clinical investigation into P-gp induction is necessary.[13] As a result of the role of P-gp and its interplay with CYP3A in drug absorption and disposition, it is important to quantitatively understand the magnitude of DDIs when the expressions of P-gp and CYP3A are upregulated by inducers.

Rifampicin is a well-established PXR agonist and is widely recognized as one of the most potent inducers of both P-gp and CYP3A.[12,14] The effect of multiple-dose rifampicin administration on the exposure of P-gp substrates has been investigated in several clinical DDI studies.[15–21] The results from the rifampicin–digoxin interaction studies showed that rifampicin treatment led to an average reduction of digoxin area under the concentration-time curve (AUC) by 15% to 30% after multiple doses, with certain individuals showing a larger reduction by more than twofold. Other P-gp substrates, such as dabigatran etexilate and talinolol, were also shown to have reduced exposures after rifampicin administration.[19,20] The induction effect was corroborated by the observation that there

was a 1.4-fold to 3.5-fold increase in P-gp protein levels in healthy subjects who received 600 mg rifampicin once daily for 10 days, as measured using immunohistochemistry and Western blot.[16]

Although the application of PBPK in predicting CYP3A4 induction has been well established,[4,22,23] the use of PBPK in predicting P-gp induction is relatively less reported. The published PBPK models for rifampicin incorporated the measured fold increase in the P-gp protein level and reasonably recovered the clinically observed magnitudes of DDIs with a number of P-gp substrates (e.g., digoxin and talinolol) when coadministered with rifampicin.[24–26] However, although it has been shown that the individual effects of CYP3A4 induction and P-gp induction on the exposure of P-gp and CYP3A4 probe substrates can be reasonably recovered by PBPK modeling, the predictability of PBPK models for the effect of simultaneous P-gp and CYP3A4 induction on P-gp-CYP3A4 dual substrates has not been investigated systematically.

Hence, the aim of this study was to perform a trend analysis of P-gp (and CYP3A4) substrates to evaluate the impact of concurrent P-gp and CYP3A4 induction by rifampicin. To this end, we have (1) collated data to develop or expand PBPK models for 12 drugs with varied degrees of CYP3A4-mediated metabolism (fraction of drug elimination through the CYP3A4-mediated pathway [fm_{CYP3A4}]) and P-gp–mediated intestinal efflux; (2) performed PBPK modeling and simulation to predict the effect of simultaneous induction of P-gp and CYP3A4 by rifampicin compared with the predictions without considering P-gp induction in the model; and (3) systematically evaluated the effects of the interplay among the key parameters such as fm_{CYP3A4}, *in vitro* intestinal P-gp–mediated intrinsic clearance ($CL_{int,T}$), and the effective intestinal passive permeability ($P_{eff,man}$) on rifampicin DDIs.

METHODS

Model-based analysis of *in vitro* P-gp kinetic data

Kinetic parameters ($CL_{int,T}$ or Michaelis–Menten constant accounting for the binding *in vitro* system [K_m] and *in vitro* maximum rate of intestinal P-gp–mediated efflux correcting for the insert growth area of the Transwell [J_{max}]) for P-gp–mediated active transport were determined by modeling *in vitro* data from bidirectional transport assays using the simcyp *in vitro* data analysis (SIVA) Toolkit (Version 4.0, Sheffield, UK).[27] Briefly, *in vitro* data were fitted to a mechanistic model consisting of three compartments representing the apical medium, cell monolayer, and basolateral medium. Active efflux mediated by P-gp is described by first-order kinetics and driven by unbound intracellular concentration. The *in vitro* data used in the model-based analysis were obtained from the literature or in-house measurements. In cases where *in vitro* data were not available, kinetic parameters for P-gp–mediated transport were estimated using *in vivo* pharmacokinetic (PK) data as indicated in the supplementary materials for the corresponding compound model (Table S1). Estimation of the relevant parameters were performed using the Nelder–Mead algorithm and weighted by reciprocal of predicted values. The representative *in vitro* modeling examples (i.e., bosutinib and crizotinib) are provided as a SIVA file in the supplementary materials.

Accounting for intestinal P-gp induction in DDI simulations

The clinical study designs of DDIs with rifampicin are summarized in Table S2. To account for the induction effect of intestinal P-gp by multiple doses of rifampicin, a 3.5-fold increase of intestinal P-gp level at steady state, as measured using Western blot,[16,26] was considered in the simulations. Briefly, a 3.5-fold increase in the relative expression factor (REF) of intestinal P-gp kinetics was incorporated into substrate models. For each DDI study, two simulations were performed to represent (1) the control phase (substrate with default P-gp REF is administered without rifampicin) and (2) the interaction phase (substrate with 3.5-fold increase in P-gp REF is administered with rifampicin). The magnitude of DDI is evaluated using the ratio of substrate AUC from Simulation 2 to that from Simulation 1 (AUC ratio) as well as the ratio of substrate maximum (peak) plasma drug concentration (C_{max}) from Simulation 2 to that from Simulation 1 (C_{max} ratio). More details about the consideration of P-gp REF in the scaling of P-gp activity are provided in the supplementary materials.

PBPK model development and evaluation

PBPK modeling and simulation were performed using the Simcyp Population-based absorption, distribution, metabolism and excretion Simulator (Version 18 Release 2, Sheffield, UK). For each DDI simulation, 10 virtual trials were performed and each trial included the same number of subjects (Sim-Healthy Volunteers) as in the corresponding clinical study. Demographic and trial design information in the simulations were matched to that of the clinical studies. When demographic information was not available, a default age range (20–50 years old) and proportion of females (50%) were used for the simulation. The initial PBPK models for the substrates were either

adopted from publications or from the Simcyp Simulator default compound library. These initial PBPK models were further developed to incorporate active transport mediated by intestinal P-gp if this was not considered in the first instance. The performance of the final model for each substrate in predicting the plasma concentration–time profile of the substrate at a clinically relevant dose was considered to be acceptable if (1) all of the observed plasma concentrations were within 5th–95th percentiles of the simulated plasma concentrations in the virtual population and (2) the simulated AUC and C_{max} values were within 0.8-fold to 1.25-fold of the observed data. For DDI predictions, the precision and bias of AUC and C_{max} ratios were assessed by the root mean square error (RMSE) and average fold error (AFE), respectively.

$$\mathrm{RMSE} = \sqrt{\frac{\sum (\text{predicted ratio} - \text{observed ratio})^2}{\text{number of predictions } (N)}}$$

$$\mathrm{AFE} = 10^{\frac{1}{n}\sum \log\left(\frac{\text{predicted ratio}}{\text{observed ratio}}\right)}.$$

Sensitivity analysis

A hypothetical sensitive P-gp substrate was designed to simulate the impact of $P_{eff,man}$ and intestinal P-gp $CL_{int,T}$ on PK parameters of the substrate (AUC, C_{max}, fraction of the dose absorbed [fa], and time to reach C_{max} [T_{max}]) after oral administration and DDI magnitude (AUC and C_{max} ratios) when it is administered with rifampicin. In addition, the effect of the interplay between P-gp $CL_{int,T}$, $fm_{CYP3A4,}$ and the hepatic extraction ratio (E_H) on the level of the estimated DDIs between the P-gp–CYP3A4 dual substrate and rifampicin was investigated using a hypothetical P-gp–CYP3A4 dual substrate. The base model of the hypothetical substrate is provided in Table S3. Data visualization was performed with MATLAB 2019b (Mathworks Inc., Natick, MA).

RESULTS

PBPK model development and validation

To evaluate the effect of P-gp induction by rifampicin on DDIs, a matrix of 12 drugs were selected, including three well-characterized sensitive P-gp substrates (digoxin, dabigatran, and talinolol), seven P-gp–CYP3A4 dual substrates (abemaciclib, acalabrutinib, bosutinib, crizotinib, naldemedine, naloxegol, and olaparib), and two P-gp–CYP3A4 dual substrates that were also inhibitors of both P-gp and CYP3A4 (quinidine and verapamil). The key PK characteristics of these substrates are summarized in Table 1. The intestinal P-gp $CL_{int,T}$ or J_{max} over K_m values incorporated in the models varied from 2.33 to 531 μl/min, whereas the fm_{CYP3A4} of these drugs ranged from 0 to 0.99. The PBPK models for digoxin, dabigatran, talinolol, and naloxegol were adopted from the literature, and their performance was validated previously against clinical PK data from multiple studies.[24,25,28] For the three P-gp sensitive substrates (digoxin, dabigatran, and talinolol), the P-gp component was further validated in previous publications using clinical DDI studies with a P-gp inhibitor/inducer.[24,26] The initial PBPK models of abemaciclib, acalabrutinib, bosutinib, naldemedine, olaparib, and quinidine were adopted from the literature and refined to incorporate P-gp–mediated efflux in the intestine.[24,29–33] The PBPK models of crizotinib, verapamil (including metabolite norverapamil), and rifampicin were from the Simcyp Simulator default compound library with minor modifications. The input parameters of the PBPK model for each drug are summarized in Table S1. All of the compound files used in the simulation are available as part of the supplementary materials. The simulated plasma concentration–time profiles following the clinically relevant dose of each drug were in good agreement with the observed data (Figure S1). The simulated PK parameters (AUC and C_{max}) were within 0.8-fold to 1.25-fold of the observed data for all compounds (Figure S2). For each drug, the simulated luminal concentration and unbound drug concentration in the enterocytes from each intestinal segment are shown in Figures S3 and S4, respectively. The unbound drug concentration in the enterocyte, as the driving concentration of first-pass metabolism and apical efflux in the gut, will lead to saturation of these processes when it is substantially higher than the K_m of these processes. The passive diffusion rate (from gut lumen to gut enterocyte) and the P-gp–mediated active efflux rate (from gut enterocyte back into gut lumen) in each intestinal region from the jejunum through to the colon are shown for each drug (Figure S5) as an indication of the relative contribution of passive permeation and active efflux to oral absorption in different regions of the intestine. The passive diffusion rate is represented by positive values, whereas the active efflux rate is represented by negative values as a counteracting process against absorption. Hence, the difference between the magnitudes of passive diffusion and active efflux indicates the sensitivity of a drug as a P-gp substrate. The intrinsic efflux clearance mediated by intestinal P-gp for each compound in the absence of rifampicin is shown in Figure S6, which exhibits substrate and intestinal region dependencies. The saturation of P-gp intrinsic clearance was observed for a number of compounds, including abemaciclib, bosutinib, crizotinib, olaparib, quinidine, verapamil, dabigatran, and talinolol. As mentioned previously, the extent of saturation was dependent on the unbound concentration of the substrate in the enterocyte compartment

TABLE 1 Key physiochemical and pharmacokinetic parameters

Drug	Log $P_{o:w}$	Compound type (pKa)	f_u	B:P	fa[a]	Fg[a]	$f_{u,gut}$	$P_{eff,man}$	Intestinal P-gp kinetics, $CL_{int,T}$ (K_m; J_{max}; RAF/REF)	fm_{CYP3A4}	Fh[a]	Intrinsic solubility (mg/ml)	Dose (mg)
Abemaciclib	3.36	Diprotic base (7.95, 4.48)	0.0557	0.84	0.91	0.84	1	2.46	35.1[b] [*0.57*[b], *20*[b], *1*]	0.91	0.67	0.0016[d]	200
Acalabrutinib	2.03	Diprotic base (5.77, 3.54)	0.026	0.787	0.94	0.95	0.026	7.72	*27.3*	0.80	0.33	0.048	100
Bosutinib	3.1	Monoprotic base (7.9)	0.063	1.2	0.74	0.97	0.063	1.51	116 [*0.58*, *67.4*, *1*]	0.99	0.66	0.02	500
Crizotinib	4.28	Diprotic base (9.4, 5.6)	0.093	1.1	0.35	0.98	0.093	0.578	43.4 [*3.8*, *165*, *1*]	0.68	0.55	0.00047[d]	250
Naldemedine	3.2	Diprotic base (7.4, 4.5)	0.063	0.6	0.69	0.998	0.063	3.16	*12*	0.72	0.93	0.227	0.2
Naloxegol	1.43	Diprotic base (9.48, 8.45)	0.958	1	0.91	0.95	1	3.5	*5*[c]	0.90	0.45	0.0566	25
Olaparib	1.55	Neutral	0.181	0.7	0.94	0.998	0.259	36.3	8.37 [*28.8*, *241*, *1*]	0.75	0.92	0.082	300
Quinidine	2.81	Diprotic base (8.8, 4.2)	0.202	0.82	0.98	0.97	1	3.47	40.6 [*0.278*, *11.3*, *1*]	0.76	0.81	0.334	332
Verapamil	4.46	Monoprotic base (8.78)	0.09	0.709	0.99	0.86	1	6.08	2.33 [*0.734*, *2.814*, *0.608*]	0.68	0.28	0.00394	120
Digoxin	1.26	Neutral	0.71	1.07	0.85	1.0	1	4.67	4.9 [*177*, *434*, *2*]	–	0.97	0.127	1
Dabigatran Etexilate	3.8	Diprotic base (6.7, 4.0)	0.07	1.26	0.1	0.66	1	4.11	531 [*2.58*, *24.9*, *55*[c]]	–	0.79	0.00466	150
Talinolol	3.15	Monoprotic base (9.43)	0.45	0.94	0.7	1.0	1	4.11	16.8 [*37*, *155*, *4*[c]]	–	0.90	0.02	100

Abbreviations: B:P, blood-to-plasma partition ratio; $CL_{int,T}$, *in vitro* intestinal P-gp–mediated intrinsic clearance (μl/min); CYP3A4, cytochrome P450 3A4; fa, fraction of dose absorbed from gut; Fg, fraction of drug that escapes intestinal first-pass metabolism; Fh, fraction of drug escaping hepatic metabolism (1 − the hepatic extraction ratio [E_H]); fm_{CYP3A4}, fraction of drug elimination through the CYP3A4-mediated pathway; f_u, fraction unbound in plasma; $f_{u,gut}$, unbound fraction in enterocyte; J_{max}, *in vitro* maximum rate of intestinal P-gp–mediated efflux correcting for the insert growth area of the Transwell (pmol/min/cm^2); K_m, Michaelis–Menten constant accounting for the binding *in vitro* system (μM); log $P_{o:w}$, log of the octanol-to-water partition coefficient; $P_{eff,man}$, effective permeability in human jejunum (10^{-4} cm/s); P-gp, P-glycoprotein; RAF/REF, relative activity or relative expression factor. Intrinsic solubility (mg/ml) at pH 7.4; dose is in mg. The P-gp kinetic parameters used in each model are in italics. The input parameters of all compound files are summarized in Table S1.

[a]Predicted by physiologically based pharmacokinetic model.

[b]Optimized.

[c]Assumed the same as the *in vitro* half-maximal inhibitory concentration (IC_{50}) in μM against P-gp.

[d]Predicted from log $P_{o:w}$ and melting point.[50]

compared with the affinity of the substrate to P-gp protein (K_m). Of the compounds that were developed using K_m and J_{max} data for P-gp kinetics, digoxin, talinolol, bosutinib, verapamil, and quinidine exhibited disproportionate systemic exposure at higher oral doses likely attributed to the saturation of intestinal P-gp. For digoxin, the previously published PBPK model successfully captured the dose–exposure nonlinearity.[25] For talinolol, bosutinib, verapamil and quinidine, the PBPK models reasonably predicted the disproportionate increase in exposure at higher oral doses of these compounds (Table S4).

Importance of considering intestinal P-gp on the prediction of PK and DDI with rifampicin

Simulations suggested that increasing passive permeability led to an increase in C_{max}, AUC, and fa as well as a decrease in T_{max}. By contrast, increasing intestinal P-gp efflux activity resulted in decreased C_{max}, AUC, and fa as well as delayed T_{max} (Figure 1a,b). When intestinal P-gp was induced by rifampicin, the simulations showed that the C_{max} and AUC ratios declined rapidly from 1 to 0.5 as P-gp $CL_{int,T}$ was increased from 0 to 20 μl/min; C_{max} and AUC ratios then gradually reached a plateau of 0.3–0.4 as P-gp $CL_{int,T}$ exceeded 100 μl/min (Figure 1c,d). In addition, $P_{eff,man}$ showed a marginal impact on the magnitude of DDI with rifampicin. Increasing the $P_{eff,man}$ value by 200-fold (from 0.5 to 10×10^{-4} cm/s) only led to a 1.4-fold change of the C_{max} ratio but had no appreciable effect on the AUC ratio (Figure 1c,d). For digoxin and talinolol, which are well-characterized P-gp substrates with relatively low intestinal P-gp $CL_{int,T}$ (5 and 16.8 μl/min, respectively), the C_{max} and AUC ratios were 0.5 to 0.7 when coadministered with rifampicin, whereas for dabigatran etexilate, a P-gp substrate with higher intestinal P-gp $CL_{int,T}$ (531 μl/min), the C_{max} and AUC ratios were 0.3 and 0.4, respectively. Furthermore, the fa of digoxin (0.7), talinolol (0.7), and dabigatran etexilate (0.1) decreased by 1.4-fold, 1.8-fold, and 2.5-fold, respectively, as a result of rifampicin-mediated P-gp induction.

Accounting for concurrent P-gp and CYP3A4 induction improved DDI prediction with rifampicin

The simulation results showed that accounting for P-gp induction in addition to CYP3A4 induction led to further decreases of AUC and C_{max} ratios (from 1.2-fold to 1.6-fold and from 1.4-fold to 1.7-fold, respectively) for seven P-gp–CYP3A4 dual substrates compared with only considering CYP3A4 induction (Figure 2). Accounting for simultaneous induction of P-gp and CYP3A4 by rifampicin improved the accuracy of DDI prediction. In comparison with considering CYP3A4 induction alone, the RMSE decreased from 0.11 to 0.06 for AUC ratios and from 0.15 to 0.10 for C_{max} ratios. The AFE were reduced from 1.93 to 1.48 for AUC ratios and from 1.54 to 1.04 for C_{max} ratios. However, for quinidine and verapamil, two well-characterized competitive P-gp inhibitors, P-gp induction by rifampicin only led to marginal changes of the AUC and C_{max} ratios, which may be attributed to the saturation of intestinal P-gp at the studied dose level. In the cases of acalabrutinib, naldemedine, and naloxegol, where P-gp activity was described by $CL_{int,T}$ rather than K_m and J_{max} because of the insufficient data for determining K_m values (e.g., solubility restrictions precluded testing high substrate concentrations in the *in vitro* assays), the slightly overpredicted C_{max} ratios with P-gp induction may be attributed largely to these models not accounting for potential saturation of intestinal P-gp activity. Furthermore, sensitivity analysis was performed to evaluate the impact of intestinal P-gp–mediated efflux clearance, fm_{CYP3A4}, and E_H on the predicted AUC and C_{max} ratios for DDIs with rifampicin (Figure 3). A general trend was shown with the analysis that the level of interaction with rifampicin was increased (AUC and C_{max} ratios became smaller) as a result of increased fm_{CYP3A4} and/or increased efflux clearance mediated by intestinal P-gp (with $P_{eff,man}$ fixed at 9.3×10^{-4} cm/s in this example). For compounds with higher intestinal P-gp efflux clearance (relative to passive permeability) and higher fm_{CYP3A4} (e.g., bosutinib), a greater reduction in oral exposure with concomitant rifampicin can be expected. As a compound is substantially extracted by hepatic CYP3A4 ($E_H > 0.7$, fm_{CYP3A4}: 0.6–1) as well as intestinal CYP3A4 (fraction of the dose that escapes intestinal first-pass metabolism [Fg] < 0.46), the change of oral exposure after rifampicin pretreatment was shown to be largely driven by CYP3A4 induction, whereas P-gp induction by rifampicin had a limited effect on drug exposure. In fact, for these compounds substantially extracted by CYP3A4, the analysis suggested that increased intestinal P-gp clearance led to a slightly lower extent of interaction with rifampicin, as more drug appeared to be absorbed in the distal region of the intestine where first-pass gut metabolism mediated by CYP3A4 was less pronounced compared with the proximal region (Figure 4). By contrast, for low hepatic extraction drugs ($E_H < 0.3$, fm_{CYP3A4}: 0.6 ~ 1) with high Fg (> 0.73), the effect of P-gp induction on the magnitude of interaction with rifampicin became more pronounced and more sensitive to the intestinal P-gp–mediated clearance.

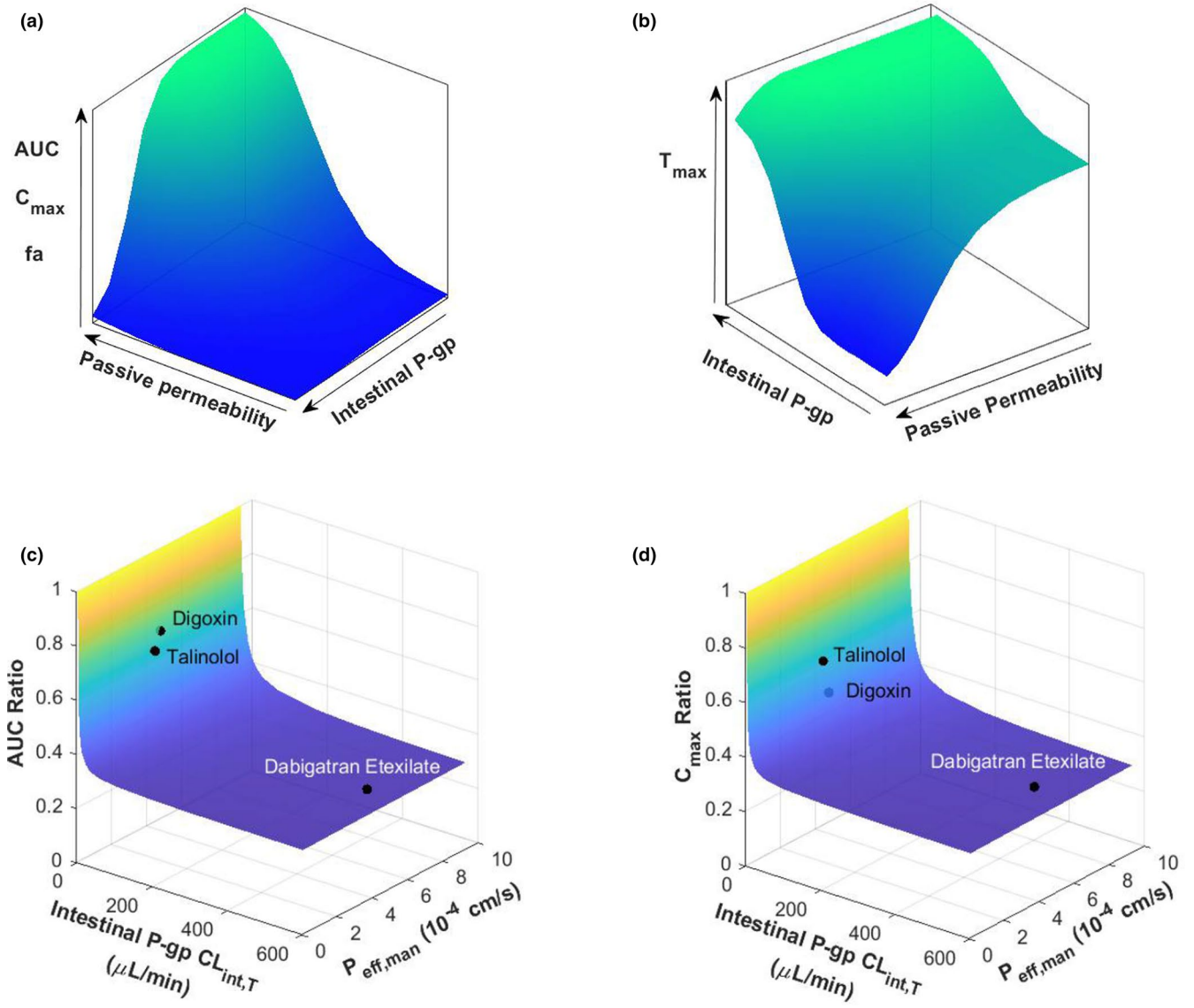

FIGURE 1 Impact of P-gp activity on predicted PK parameters and drug–drug interactions. (a and b) Impact of passive permeability and $CL_{int,T}$ on PK parameters (AUC, C_{max}, overall fa, and T_{max}) of the substrate. The direction of the arrow indicates increase of the parameter. (c and d) Impact of $P_{eff,man}$ and $CL_{int,T}$ on the interaction between rifampicin and pure P-gp substrates. The data points represent the observed AUC and C_{max} ratios of digoxin, talinolol, and dabigatran etexilate with or without the presence of multiple doses of rifampicin. AUC, area under the concentration-time curve; $CL_{int,T}$, *in vitro* intestinal P-gp–mediated intrinsic clearance; C_{max}, maximum (peak) plasma drug concentration; fa, fraction of the dose absorbed; $P_{eff,man}$, effective intestinal passive permeability; P-gp, P-glycoprotein; PK, pharmacokinetic; T_{max}, time to reach C_{max}

DISCUSSION

In the present study, we have evaluated the effect of multiple doses of rifampicin on the systemic exposure of a number of P-gp–CYP3A4 dual substrates using the PBPK modeling approach. The primary focus was to investigate the effect of considering concurrent induction of P-gp and CYP3A4 by rifampicin on the predicted levels of interaction compared with that of considering CYP3A4 induction alone. The simulation results revealed that considering both P-gp and CYP3A4 induction by rifampicin led to decreased bias and increased precision for the predicted AUC and C_{max} ratios of P-gp–CYP3A4 dual substrates in the presence and absence of multiple doses of rifampicin pretreatment compared with the simulations without P-gp induction.

Intestinal P-gp and CYP3A4 are functionally synergistic in limiting the systemic exposure of orally administered drugs. For P-gp–CYP3A4 dual substrates, drug molecules entered into the gut enterocytes can be extruded back into the gut lumen and become available for reabsorption. As drug molecules undergo this efflux and reabsorption cycle, they are more likely to be metabolized as the exposure of drug molecules to intestinal CYP3A4

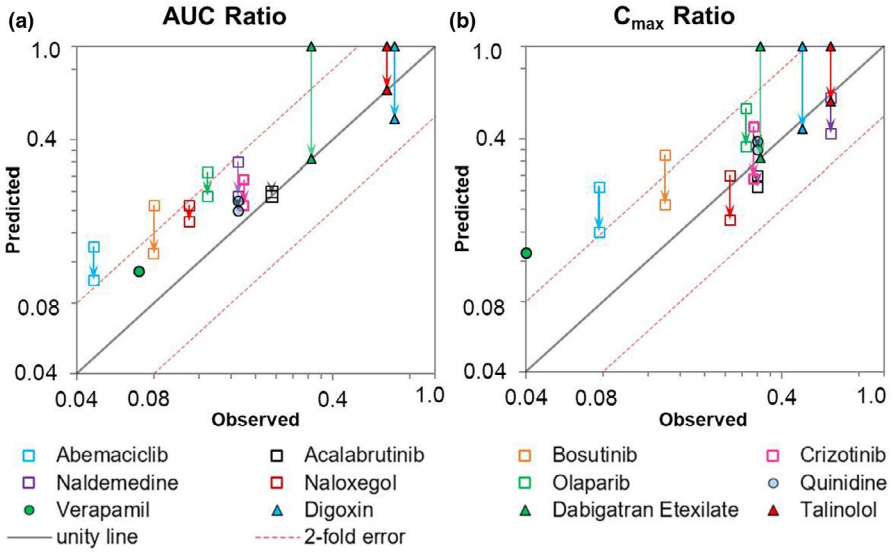

FIGURE 2 Predicted versus observed (a) AUC and (b) C_{max} ratios with or without the presence of multiple doses of rifampicin. The starting point of the arrow indicates the AUC and C_{max} ratios predicted without considering P-gp induction by rifampicin (CYP3A4 induction only). The end of the arrow indicates the AUC and C_{max} ratios predicted with CYP3A4 induction and a 3.5-fold induction of intestinal P-gp. Solid and dashed lines represent unity and 2-fold error, respectively. AUC, area under the concentration-time curve; C_{max}, maximum (peak) plasma drug concentration; CYP3A4, cytochrome P450 3A4; P-gp, P-glycoprotein

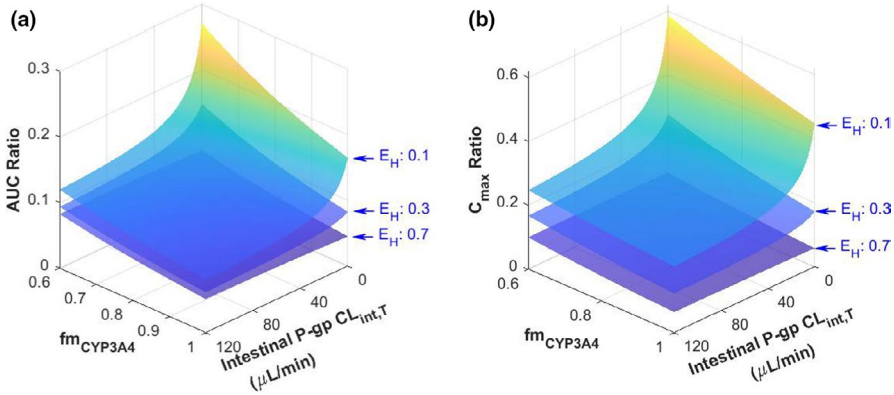

FIGURE 3 Impact of intestinal P-gp $CL_{int,T}$, fm_{CYP3A4}, and E_H on drug–drug interaction prediction. The simulated (a) AUC and (b) C_{max} ratios of P-gp–CYP3A4 dual substrate with or without the presence of multiple doses of rifampicin. AUC, area under the concentration-time curve; $CL_{int,T}$, *in vitro* intestinal P-gp–mediated intrinsic clearance; C_{max}, maximum (peak) plasma drug concentration; CYP3A4, cytochrome P450 3A4; E_H, hepatic extraction ratio; fm_{CYP3A4}, fraction of drug elimination through the CYP3A4-mediated pathway; P-gp, P-glycoprotein

is increased. Furthermore, P-gp decreases the intracellular concentration of the drug in the enterocytes, reducing the chance of CYP3A4 saturation. In addition to the functional synergy, P-gp and CYP3A4 are also shown to be coregulated by the nuclear receptors PXR and CAR and therefore can be upregulated by the agonists of these nuclear receptors.[12] Rifampicin, a well-known PXR agonist, has been shown to induce P-gp and CYP3A4 simultaneously. Hence, it is important to consider the impact of rifampicin on both P-gp and CYP3A4, especially for the assessment of DDIs when rifampicin is administered concomitantly with P-gp–CYP3A4 dual substrates. In the present study, we showed that although the initial rifampicin PBPK model (without considering P-gp induction) was validated extensively for its predictive performance for CYP3A4 induction in previous publications, there was a tendency of the initial model to underestimate the magnitudes of DDIs with P-gp–CYP3A4 dual substrates. To account for P-gp induction, a 3.5-fold increase of the P-gp protein level at steady state, which was measured by Western blot in healthy volunteers following multiple administrations of rifampicin (600 mg once daily for 10 days),[16] was incorporated in the PBPK models, resulting in successfully recovering the observed AUC and C_{max}

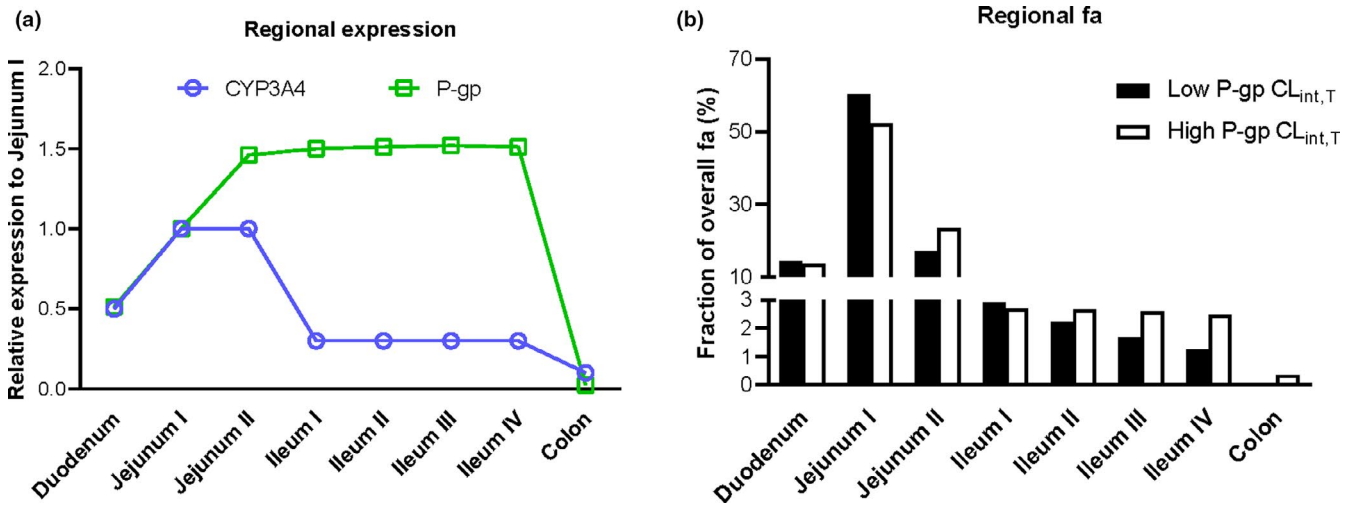

FIGURE 4 (a) Relative expression of P-gp and CYP3A4 in intestine and (b) impact of P-gp intrinsic clearance on the fa in each intestinal segment. $CL_{int,T}$, *in vitro* intestinal P-gp–mediated intrinsic clearance; CYP3A4, cytochrome P450 3A4; fa, fraction of the dose absorbed; P-gp, P-glycoprotein

ratios for P-gp probe substrates as well as P-gp–CYP3A4 dual substrates.

For an investigational drug that is substantially (>25%) metabolized by CYP3A, the assessment of the impact of CYP3A induction on drug exposure is required by multiple regulatory agencies.[13,34,35] Rifampicin is one of the most potent inducers of CYP3A4 and is extensively used in prospective DDI studies to investigate the effect of CYP3A4 induction. The findings from the DDI studies with rifampicin and strong CYP3A4 inhibitors (ketoconazole or itraconazole) are often used to validate and/or refine fm_{CYP3A4} for a given substrate in PBPK modeling.[28,30,31,33,36] Thereafter, the substrate model is considered as validated for making prospective predictions of untested scenarios (e.g., DDIs with moderate/weak inhibitors or inducers). However, such a paradigm is sometimes confounded by the experience that PBPK models tend to underpredict DDIs with rifampicin.[37,38] Such underprediction may have contributed to less regulatory clarity about the acceptability of PBPK in this area[39] and also highlighted the need to further refine the rifampicin model to account for additional induction mechanisms such as transporter induction.[37] In the case of P-gp–CYP3A4 dual substrates, it has been shown that despite fm_{CYP3A4} being validated or refined using DDIs with strong CYP3A4 inhibitors, there was a tendency to underestimate the interaction with multiple doses of rifampicin if P-gp induction was not considered. Hence, to increase the confidence in prospective prediction of DDIs with other perpetrators, it is important to differentiate the contributions of P-gp and CYP3A4 for P-gp–CYP3A4 dual substrates and account for P-gp induction in the DDI simulations with rifampicin. During drug development, it is recommended by the US FDA that most investigational drugs should be evaluated *in vitro* to determine whether they are P-gp substrates unless they are highly permeable and highly soluble. If the efflux ratio (ER) of a drug determined from *in vitro* assay meets certain criteria, a clinical DDI study should be considered based on the drug's safety margin, therapeutic index, and likely concomitant drugs that are known P-gp inhibitors.[13] In this case, it is advisable to generate more detailed kinetic data ($CL_{int,T}$ or K_m and J_{max}) other than ER as inputs to PBPK models to predict the likely magnitude of DDI when a P-gp substrate or P-gp–CYP3A4 dual substrate is coadministered with P-gp inhibitors/inducers. To address the limitations of the conventional approach that estimates P-gp kinetic data using the nominal drug concentration in the donor chamber of the *in vitro* transport system,[40] the use of *in vitro* modeling that features a dynamic and mechanistic representation of the *in vitro* transport assays has been increasingly adopted in recent years for estimating more intrinsic estimates of P-gp kinetics by accounting for active transport, passive diffusion, and relevant driving concentration of P-gp–mediated efflux in *in vitro* systems.[24,40,41]

In principle, P-gp expression can be induced by rifampicin in multiple tissues, including the intestine, liver, kidney, and brain. Nevertheless, it has been shown that the effect of rifampicin on the systemic exposure of P-gp substrates can be explained predominantly by P-gp induction in the intestine, whereas the induction of hepatic and renal P-gp has limited impact on the systemic exposure of P-gp substrates.[12] Hence, the present study primarily focused on the induction of intestinal P-gp by rifampicin. However, it should be noted that the exact mechanism underlying the differential effect of P-gp induction in different tissues still remains unclear. Therefore, it is advisable

to consider whether an inducer modulates P-gp to different extents in each organ and specify input parameters to describe the induction effects in these organs accordingly when developing inducer PBPK models using the approach described herein.

The sensitivity analysis presented in the current study suggested fm_{CYP3A4} and intestinal P-gp $CL_{int,T}$ as the main substrate characteristics that determined the level of interaction with rifampicin. This is also reflected in the observed data set that AUC and C_{max} ratios of the investigated compounds varied by approximately 4.9-fold and 15.5-fold, respectively, possibly because of the wide range of fm_{CYP3A4} and $CL_{int,T}$ of intestinal P-gp for these compounds. Although the importance of accurate fm_{CYP3A4} measurements has been widely recognized in this field, these results further pointed out the importance of reliable and detailed estimates for intestinal P-gp activity in DDI predictions. To increase the robustness of the P-gp parameters, an *in vitro* modeling approach (SIVA Toolkit) was applied in this study to estimate K_m and J_{max} where possible as P-gp saturation may offset the effect of P-gp induction by rifampicin. In cases where insufficient *in vitro* data precluded the estimation of K_m and J_{max}, $CL_{int,T}$ was estimated as the alternative input. In principle, the P-gp and CYP3A4 components of the substrate model should be individually validated using clinical DDI data before moving forward to predict the combined effect of P-gp and CYP3A4 induction. Although the assessment of fraction metabolized by CYP3A (fm_{CYP3A}) for a CYP3A4 substrate using strong index inhibitor is a widely accepted approach, applying the same strategy to validate P-gp and CYP3A4 components separately for a P-gp–CYP3A4 dual substrate model is not straightforward as most clinical inhibitors (e.g., ketoconazole, itraconazole) coadministered with these P-gp–CYP3A4 dual substrates could inhibit both P-gp and CYP3A4. Nevertheless, in cases where P-gp activity is saturated by the substrate itself, DDI studies with such inhibitors may be used to validate the CYP3A4 component separately. To demonstrate this point, the quinidine–verapamil DDI study reported by Edwards et al.[42] was simulated where the observed clearance ratios were reasonably recovered (observed vs. predicted clearance ratios were 0.69 ± 0.05 vs. 0.61 ± 0.09 with 80 mg verapamil pretreatment and 0.65 ± 0.07 vs. 0.56 ± 0.09 with 120 mg verapamil pretreatment). The simulated P-gp intrinsic clearance using K_m and J_{max} inputs revealed that intestinal P-gp was saturated by quinidine itself at the therapeutic dose (322 mg free base); hence, the DDI is predominantly driven by a mechanism-based inhibition of CYP3A4 mediated by verapamil.

The CYP3A4 induction parameters of the default rifampicin model (maximal fold induction of CYP3A4 over vehicle [Ind_{max_CYP3A4}] = 16, drug concentration that supports half maximal induction of CYP3A4 [$IndC_{50\_CYP3A4}$] = 0.32, unbound fraction of drug in enterocytes [$f_{u,gut}$] = 1) have been validated extensively using clinical DDI studies with a large number of CYP3A4 substrates.[4,22,23] An alternative set of CYP3A4 induction parameters (Ind_{max_CYP3A4} = 30.6, $IndC_{50\_CYP3A4}$ = 0.32, $f_{u,gut}$ = 0.116), which were previously used as a worst case assessment of DDI liability for metabolically stable CYP3A4 substrates, further improved the predictions for some compounds such as bosutinib by simulating a stronger induction of CYP3A4 (Figure S7). Although bosutinib is predominantly metabolized by CYP3A4 ($f_{m,CYP3A4} \approx 1$), such improvement should be interpreted with caution as rifampicin is also shown to induce other proteins such as CYP1A2, CYP2B6, CYP2C8, CYP2C9, UDP glucuronosyltransferase (UGT)1A1, and possibly organic anion transporting polypeptide (OATP)1B1,[15,43–48] which may account for the underestimation of DDIs with the default rifampicin model when their involvement, if any, is not considered in the substrate model. Hence, further investigation is warranted to identify whether metabolic pathways mediated by non-CYP enzymes as well as CYP enzymes other than CYP3A4 were involved in the metabolism of the substrates and contributed to the interaction with rifampicin.

One of the limitations of this study is that the current model does not account for the time dependency of P-gp induction, as the induction effect was considered in the simulations by increasing the P-gp level based on the observed fold induction of P-gp at steady state. Although this had a limited impact on the simulations in the present study as the substrates were administered after the induction effect reached steady state following multiple doses of rifampicin, dynamic models that take into consideration the rates of P-gp synthesis and degradation are required to fully understand the time dependency of P-gp induction, such as the effect of dose staggering and the level of DDIs before steady state is reached.

In summary, although challenges remain in differentiating the effects of P-gp and CYP3A4 inductions on oral drug exposure of their substrates, the present study demonstrated the utility of the PBPK modeling approach to predict the effect of simultaneous P-gp and CYP3A4 induction on the exposure of P-gp–CYP3A4 dual substrates. According to the European Medicines Agency guidance, a data set of 8–10 compounds is indicative of a sufficient number of compounds to qualify a specific system model of a PBPK platform,[49] hence the data set presented in the present study provides a valuable aid in understanding the combined effect of P-gp and CYP3A induction during drug development. The PBPK models described herein, when informed by robust *in vitro* and clinical data, can help in the assessment of DDI potentials for investigational drugs as P-gp and CYP3A substrates or inducers.

ACKNOWLEDGMENTS

The authors acknowledge Emi Yamaguchi, Chester Costales, Emi Kimoto, and Manthena V. Varma (Pharmacokinetics, Dynamics & Metabolism, Pfizer Worldwide Research & Development, Groton, CT) for providing *in vitro* Caco-2 data.

CONFLICT OF INTEREST

X.P., S.N., and M.Z. are full-time employees of Certara UK Limited. V.P.R. and S.Y. are full-time employees and hold shares of AstraZeneca and Pfizer, respectively.

AUTHOR CONTRIBUTIONS

X.P., S.Y., S.N., M.Z., and V.P.R. wrote the manuscript. X.P., S.Y., S.N., and V.P.R. designed the research. X.P., S.Y., S.N., M.Z., and V.P.R. performed the research. X.P., S.Y., S.N., M.Z., and V.P.R. analyzed the data.

ORCID

Xian Pan https://orcid.org/0000-0003-2418-5970
Shinji Yamazaki https://orcid.org/0000-0001-7112-2812
Sibylle Neuhoff https://orcid.org/0000-0001-8809-1960
Mian Zhang https://orcid.org/0000-0001-7813-3442
Venkatesh Pilla Reddy https://orcid.org/0000-0002-7786-4371

REFERENCES

1. Luzon E, Blake K, Cole S, Nordmark A, Versantvoort C, Berglund EG. Physiologically based pharmacokinetic modeling in regulatory decision-making at the European Medicines Agency. *Clin Pharmacol Ther*. 2017;102:98-105.
2. Rowland M, Lesko L, Rostami-Hodjegan A. physiologically based pharmacokinetics is impacting drug development and regulatory decision making. *CPT: Pharmacometrics Syst Pharmacol*. 2015;4(6):313-315.
3. Zhang X, Yang Y, Grimstein M, et al. Application of PBPK modeling and simulation for regulatory decision making and its impact on US prescribing information: an update on the 2018–2019 submissions to the US FDA's office of clinical pharmacology. *J Clin Pharmacol*. 2020;60:S160-S178.
4. Bolleddula J, Ke A, Yang H, Prakash C. PBPK modeling to predict drug-drug interactions of ivosidenib as a perpetrator in cancer patients and qualification of the Simcyp platform for CYP3A4 induction. *CPT: Pharmacometrics Syst Pharmacol*. 2021;10(6):577-588.
5. Taskar KS, et al. Physiologically-based pharmacokinetic models for evaluating membrane transporter mediated drug–drug interactions: current capabilities, case studies, future opportunities, and recommendations. *Clin Pharmacol Ther*. 2020;107:1082-1115.
6. Fromm MF. P-glycoprotein: a defense mechanism limiting oral bioavailability and CNS accumulation of drugs. *Int J Clin Pharmacol Ther*. 2000;38:69-74.
7. Fromm MF. Importance of P-glycoprotein at blood–tissue barriers. *Trends Pharmacol Sci*. 2004;25:423-429.
8. Tanigawara Y. Role of P-glycoprotein in drug disposition. *Ther Drug Monit*. 2000;22:137-140.
9. Lown KS, Mayo RR, Leichtman AB, et al. Role of intestinal P-glycoprotein (mdr1) in interpatient variation in the oral bioavailability of cyclosporine. *Clin Pharmacol Ther*. 1997;62:248-260.
10. Zhang Y, Guo X, Lin ET, Benet LZ. Overlapping substrate specificities of cytochrome P450 3A and P-glycoprotein for a novel cysteine protease inhibitor. *Drug Metab Dispos*. 1998;26:360-366.
11. Zaccara G, Perucca E. Interactions between antiepileptic drugs, and between antiepileptic drugs and other drugs. *Epileptic Disord*. 2014;16:409-431.
12. Elmeliegy M, Vourvahis M, Guo C, Wang DD. Effect of P-glycoprotein (P-gp) inducers on exposure of P-gp substrates: review of clinical drug–drug interaction studies. *Clin Pharmacokinet*. 2020;59:699-714.
13. Administration *In vitro drug interaction studies—cytochrome P450 enzyme-and transporter-mediated Drug Interactions*. https://www.fda.gov/regulatory-information/search-fda-guidance-documents/vitro-drug-interaction-studies-cytochrome-p450-enzyme-and-transporter-mediated-drug-interactions. Published 2020. Accessed October 4, 2021.
14. Ohnhaus E, Gerber-Taras E, Park B. Enzyme-inducing drug combinations and their effects on liver microsomal enzyme activity in man. *Eur J Clin Pharmacol*. 1983;24:247-250.
15. Zamek-Gliszczynski MJ, et al. Intestinal P-gp and putative hepatic OATP1B induction: ITC perspective on drug development implications. *Clin Pharmacol Ther*. 2020;109:55–64.
16. Greiner B, Eichelbaum M, Fritz P, et al. The role of intestinal P-glycoprotein in the interaction of digoxin and rifampin. *J Clin Invest*. 1999;104:147-153.
17. Gault H, Longerich L, Dawe M, Fine A. Digoxin-rifampin interaction. *Clin Pharmacol Ther*. 1984;35:750-754.
18. Acocella G. Clinical pharmacokinetics of rifampicin. *Clin Pharmacokinet*. 1978;3:108-127.
19. Westphal K. Induction of P-glycoprotein by rifampin increases intestinal secretion of talinolol in human beings: a new type of drug/drug interaction. *Clin Pharmacol Ther*. 2000;68:345-355.
20. Härtter S, Koenen-Bergmann M, Sharma A, et al. Decrease in the oral bioavailability of dabigatran etexilate after co-medication with rifampicin. *Br J Clin Pharmacol*. 2012;74:490-500.
21. Lutz JD, Kirby BJ, Wang LU, et al. Cytochrome P450 3A induction predicts P-glycoprotein induction; part 1: establishing induction relationships using ascending dose rifampin. *Clin Pharmacol Ther*. 2018;104:1182-1190.
22. De Zwart L, Snoeys J, De Jong J, Sukbuntherng J, Mannaert E, Monshouwer M. Ibrutinib dosing strategies based on interaction potential of CYP3A4 perpetrators using physiologically based pharmacokinetic modeling. *Clin Pharmacol Ther*. 2016;100:548-557.
23. Almond LM, Mukadam S, Gardner I, et al. Prediction of drug-drug interactions arising from CYP3A induction using a physiologically based dynamic model. *Drug Metab Dispos*. 2016;44:821-832.
24. Yamazaki S, Costales C, Lazzaro S, Eatemadpour S, Kimoto E, Varma MV. Physiologically-based pharmacokinetic modeling approach to predict rifampin-mediated intestinal p-glycoprotein induction. *CPT: Pharmacometrics Syst Pharmacol*. 2019;8:634-642.
25. Neuhoff S, Yeo KR, Barter Z, Jamei M, Turner DB, Rostami-Hodjegan A. Application of permeability-limited physiologically-based pharmacokinetic models: part I-digoxin pharmacokinetics incorporating P-glycoprotein-mediated efflux. *J Pharm Sci*. 2013;102:3145-3160.
26. Neuhoff S, Yeo KR, Barter Z, Jamei M, Turner DB, Rostami-Hodjegan A. Application of permeability-limited

physiologically-based pharmacokinetic models: part II - prediction of P-glycoprotein mediated drug-drug interactions with digoxin. *J Pharm Sci*. 2013;102:3161-3173.
27. *The Simcyp™ In Vitro Data Analysis (SIVA) Toolkit*. www.certara.com/software/simcyp-in-vitro-data-analysis-toolkit-siva/. Accessed October 4, 2021.
28. Zhou D, Bui K, Sostek M, Al-Huniti N. Simulation and prediction of the drug-drug interaction potential of naloxegol by physiologically based pharmacokinetic modeling. *CPT Pharmacometrics Syst Pharmacol*. 2016;5:250-257.
29. Posada MM, Morse BL, Turner PK, Kulanthaivel P, Hall SD, Dickinson GL. Predicting clinical effects of CYP3A4 modulators on abemaciclib and active metabolites exposure using physiologically based pharmacokinetic modeling. *J Clin Pharmacol*. 2020;60(7):915-930.
30. Zhou D, et al. Evaluation of the drug-drug interaction potential of acalabrutinib and its active metabolite, ACP-5862, using a physiologically-based pharmacokinetic modeling approach. *CPT Pharmacometrics Syst Pharmacol*. 2019;8:489-499.
31. Yamazaki S, Loi CM, Kimoto E, Costales C, Varma MV. Application of physiologically based pharmacokinetic modeling in understanding bosutinib drug-drug interactions: importance of intestinal P-glycoprotein. *Drug Metab Dispos*. 2018;46:1200-1211.
32. Center for Drug Evaluation and Research, Food and Drug Administration. *NDA-208854 (Naldemedine, SYMPROIC®) clinical pharmacology and biopharmaceutics review*. www.accessdata.fda.gov/drugsatfda_docs/nda/2017/208854Orig1s000ClinPharmR.pdf. Published 2016. Accessed October 4, 2021.
33. Pilla Reddy V, Bui K, Scarfe G, Zhou D, Learoyd M. Physiologically based pharmacokinetic modeling for olaparib dosing recommendations: bridging formulations, drug interactions, and patient populations. *Clin Pharmacol Ther*. 2019;105:229-241.
34. *European Medicines Agency. Guideline on the investigation of drug interactions.*. https://www.ema.europa.eu/en/documents/scientific-guideline/guideline-investigation-drug-interactions-revision-1_en.pdf. Published 2012. Accessed October 4, 2021.
35. Pharmaceuticals and Medical Devices Agency. *Guideline on Drug Interaction for Drug Development and Appropriate Provision of Information*. 2018. https://www.pmda.go.jp/files/000228122.pdf. Accessed April 10, 2021.
36. Yamazaki S, Johnson TR, Smith BJ. Prediction of drug-drug interactions with crizotinib as the CYP3A substrate using a physiologically based pharmacokinetic model. *Drug Metab Dispos*. 2015;43:1417-1429.
37. Wagner C, Pan Y, Hsu V, Sinha V, Zhao P. Predicting the effect of CYP3A inducers on the pharmacokinetics of substrate drugs using physiologically based pharmacokinetic (PBPK) modeling: an analysis of PBPK submissions to the US FDA. *Clin Pharmacokinet*. 2016;55:475-483.
38. US Food and Drug Administration workshop. Physiologically based pharmacokinetic modeling & simulation in OCP submissions: case studies. www.fda.gov/media/134177/download. Published 2019. Accessed September 13, 2021.
39. European Medicines Agency. *Overview of comments received on 'Guideline on the qualification and reporting of physiologically based pharmacokinetic (PBPK) modelling and simulation' (EMA/CHMP/458101/2016)*. www.ema.europa.eu/en/documents/comments/overview-comments-received-guideline-qualification-reporting-physiologically-based-pharmacokinetic/chmp/458101/2016_en.pdf. Published 2020. Accessed October 4, 2021.
40. Tachibana T, Kitamura S, Kato M, et al. Model analysis of the concentration-dependent permeability of P-gp substrates. *Pharm Res*. 2010;27:442-446.
41. Riede J, Umehara K-I, Schweigler P, et al. Examining P-gp efflux kinetics guided by the BDDCS–Rational selection of in vitro assay designs and mathematical models. *Eur J Pharm Sci*. 2019;132:132-141.
42. Edwards DJ, Lavoie R, Beckman H, Blevins R, Rubenfire M. The effect of coadministration of verapamil on the pharmacokinetics and metabolism of quinidine. *Clin Pharmacol Ther*. 1987;41:68-73.
43. Dixit V, Hariparsad N, Li F, Desai P, Thummel KE, Unadkat JD. Cytochrome P450 enzymes and transporters induced by anti-human immunodeficiency virus protease inhibitors in human hepatocytes: implications for predicting clinical drug interactions. *Drug Metab Dispos*. 2007;35:1853-1859.
44. Dixit V, Moore A, Tsao H, Hariparsad N. Application of micropatterned cocultured hepatocytes to evaluate the inductive potential and degradation rate of major xenobiotic metabolizing enzymes. *Drug Metab Dispos*. 2016;44:250-261.
45. Kirby BJ, Collier AC, Kharasch ED, et al. Complex drug interactions of HIV protease inhibitors 2: in vivo induction and in vitro to in vivo correlation of induction of cytochrome P450 1A2, 2B6, and 2C9 by ritonavir or nelfinavir. *Drug Metab Dispos*. 2011;39:2329-2337.
46. Buckley DB, Wiegand CM, Prentiss PL, Fahmi OA. *Time-Course of Cytochrome P450 (CYP450) Induction in Cultured Human Hepatocytes: Evaluation of Activity and mRNA Expression Profiles for Six Inducible CYP450 Enzymes*. In ISSX.
47. Smith CM, Faucette SR, Wang H, LeCluyse EL. Modulation of UDP-glucuronosyltransferase 1A1 in primary human hepatocytes by prototypical inducers. *J Biochem Mol Toxicol*. 2005;19:96-108.
48. Williamson B, Dooley KE, Zhang Y, Back DJ, Owen A. Induction of influx and efflux transporters and cytochrome P450 3A4 in primary human hepatocytes by rifampin, rifabutin, and rifapentine. *Antimicrob Agents Chemother*. 2013;57:6366-6369.
49. European Medicines Agency. *Guideline on the reporting of physiologically based pharmacokinetic (PBPK) modelling and simulation*. https://www.ema.europa.eu/en/documents/scientific-guideline/guideline-reporting-physiologically-based-pharmacokinetic-pbpk-modelling-simulation_en.pdf. Published 2018. Accessed October 4, 2021.
50. Jain N, Yalkowsky SH. Estimation of the aqueous solubility I: application to organic nonelectrolytes. *J Pharm Sci*. 2001;90:234-252.

SUPPORTING INFORMATION

Additional supporting information may be found in the online version of the article at the publisher's website.

How to cite this article: Pan X, Yamazaki S, Neuhoff S, Zhang M, Pilla Reddy V. Unraveling pleiotropic effects of rifampicin by using physiologically based pharmacokinetic modeling: Assessing the induction magnitude of P-glycoprotein–cytochrome P450 3A4 dual substrates. *CPT Pharmacometrics Syst Pharmacol*. 2021;10:1485–1496. doi:10.1002/psp4.12717